

Supplementary Material

Structural, Spectroscopic and Electrochemical Characterisation of Semi-conducting, Solvated $[\text{Pt}(\text{NH}_3)_4](\text{TCNQ})_2 \cdot (\text{DMF})_2$ and Non-solvated $[\text{Pt}(\text{NH}_3)_4](\text{TCNQ})_2$

Jinzhen Lu,^{A,G} Ayman Nafady,^{A,B,G} Brendan F. Abrahams,^C Muhammad Abdulhamid,^{A,D}

Bjorn Winther-Jensen,^{E,F} Alan M Bond,^{A,H} and Lisandra L Martin^{A,H}

^A School of Chemistry, Monash University, Clayton, Victoria, 3800, Australia

^B Current address: Chemistry Department, College of Science, King Saud University, Riyadh, Saudi Arabia

^C School of Chemistry, University of Melbourne, Victoria, 3010, Australia

^D Current address: Department of Applied Physics, Chalmers University of Technology, Göteborg, Sweden

^E Materials Engineering, Monash University, Clayton, Victoria, 3800, Australia

^F Current address: Department of Advanced Science and Engineering, Waseda University, Tokyo 169-8555, Japan

^G Joint first authors with an equal contribution.

^H Corresponding authors: Email: Alan.Bond@monash.edu and Lisa.Martin@monash.edu

Table of contents

Figure S1: Experimental and calculated powder XRD diffraction pattern of $[(\text{NH}_3)_4\text{Pt}](\text{TCNQ})_2$ (2)	S3
Figure S2. FTIR spectra of $[\text{Pt}(\text{NH}_3)_4](\text{TCNQ})_2 \cdot (\text{DMF})_2$ (1) and $[\text{Pt}(\text{NH}_3)_4](\text{TCNQ})_2$ (2)	S4
Figure S3. UV-vis spectra of dissolved 1 , 2 , LiTCNQ and neutral TCNQ in CH_3CN	S5
Figure S4. Solution phase electrochemistry of 2	S6
Figure S5. Raman spectra of TCNQ and 2 obtained electrochemically	S7
Figure S6. Voltammetric evidence for nucleation/growth mechanism	S8
Figure S7. Chronoamperometric evidence for nucleation/growth mechanism	S9
Figure S8. ^1H NMR spectrum of a supernatant solution after 1 is soaked in D_2O	S10
Figure S9. FTIR spectrum of 1 after being soaked in D_2O	S11
Table S1. Catalytic properties for several $\text{TCNQ}(\text{F}_4)^{0/1-/2-}$ derived materials	S12
Supplementary References	S13

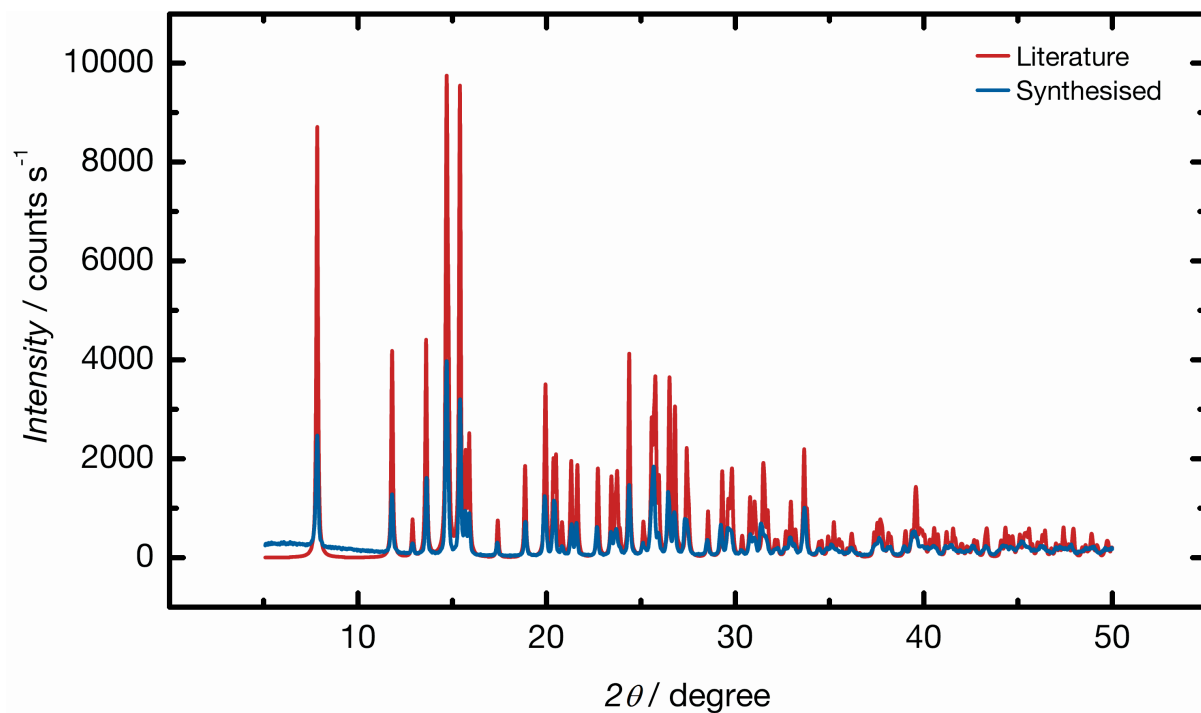
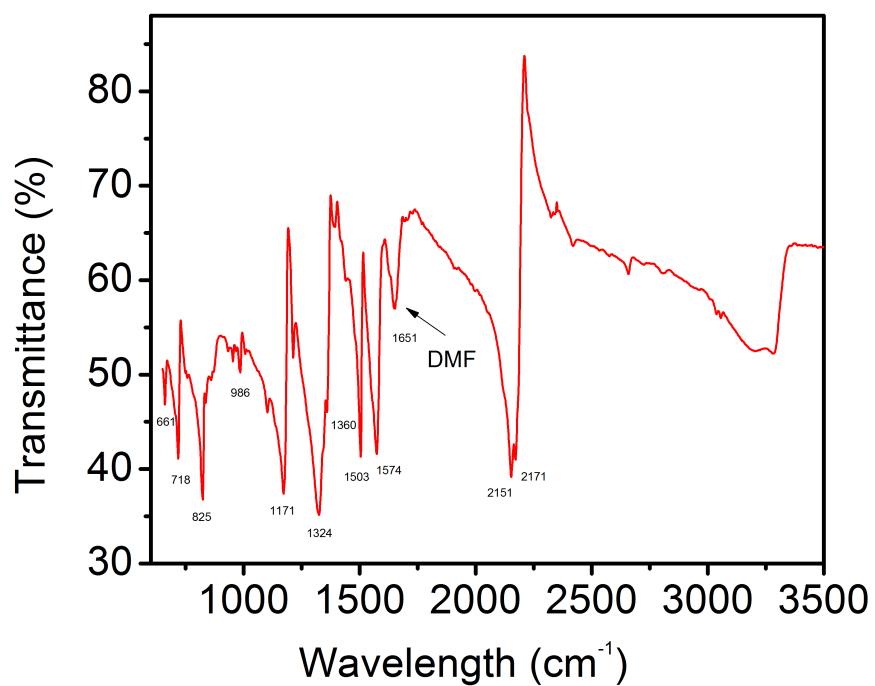


Figure S1: Comparison of X-ray powder diffraction pattern of [Pt(NH₃)₄](TCNQ)₂ (**2**) (blue) and that calculated from the structure of [Pt(NH₃)₄](TCNQ)₂ (red).^{S1}

a)



b)

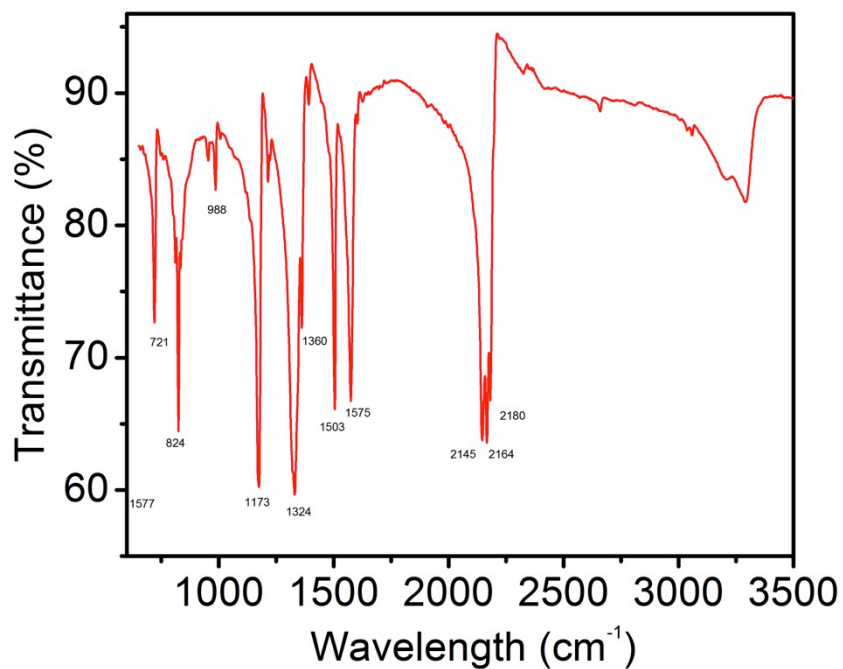


Figure S2: FTIR spectrum of solid (a) $[\text{Pt}(\text{NH}_3)_4](\text{TCNQ})_2 \cdot (\text{DMF})_2$ (**1**) and solid (b) $[\text{Pt}(\text{NH}_3)_4](\text{TCNQ})_2$ (**2**)

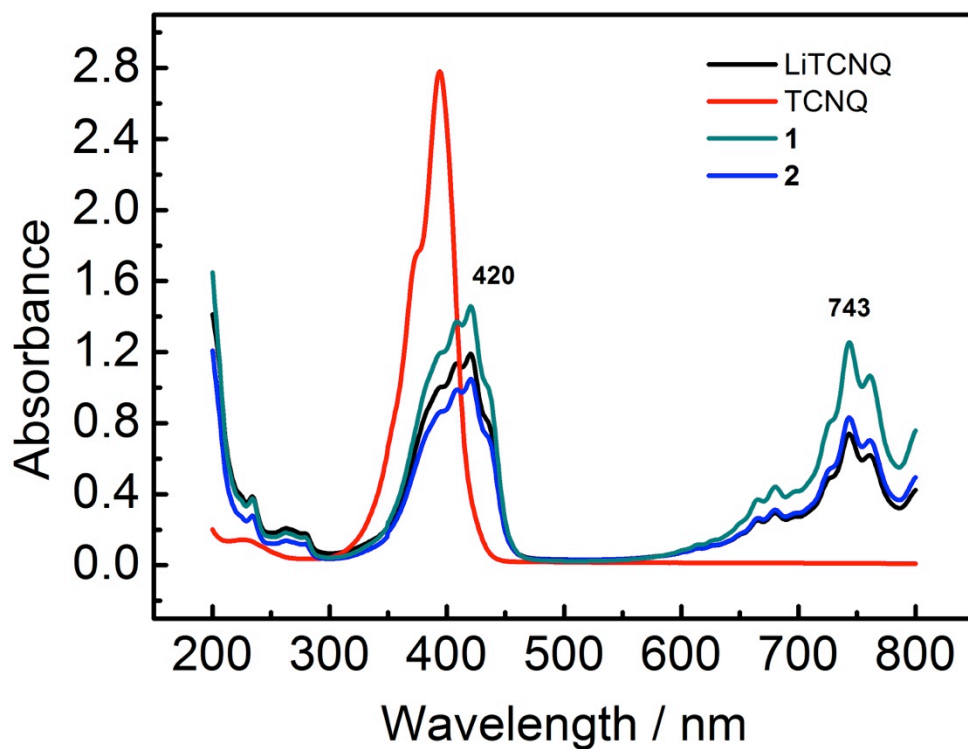


Figure S3: UV-vis spectra of dissolved $[\text{Pt}(\text{NH}_3)_4](\text{TCNQ})_2 \cdot (\text{DMF})_2$ (**1**), $[\text{Pt}(\text{NH}_3)_4](\text{TCNQ})_2$ (**2**), compared with dissolved TCNQ^{1-} (from LiTCNQ) and neutral TCNQ in CH_3CN

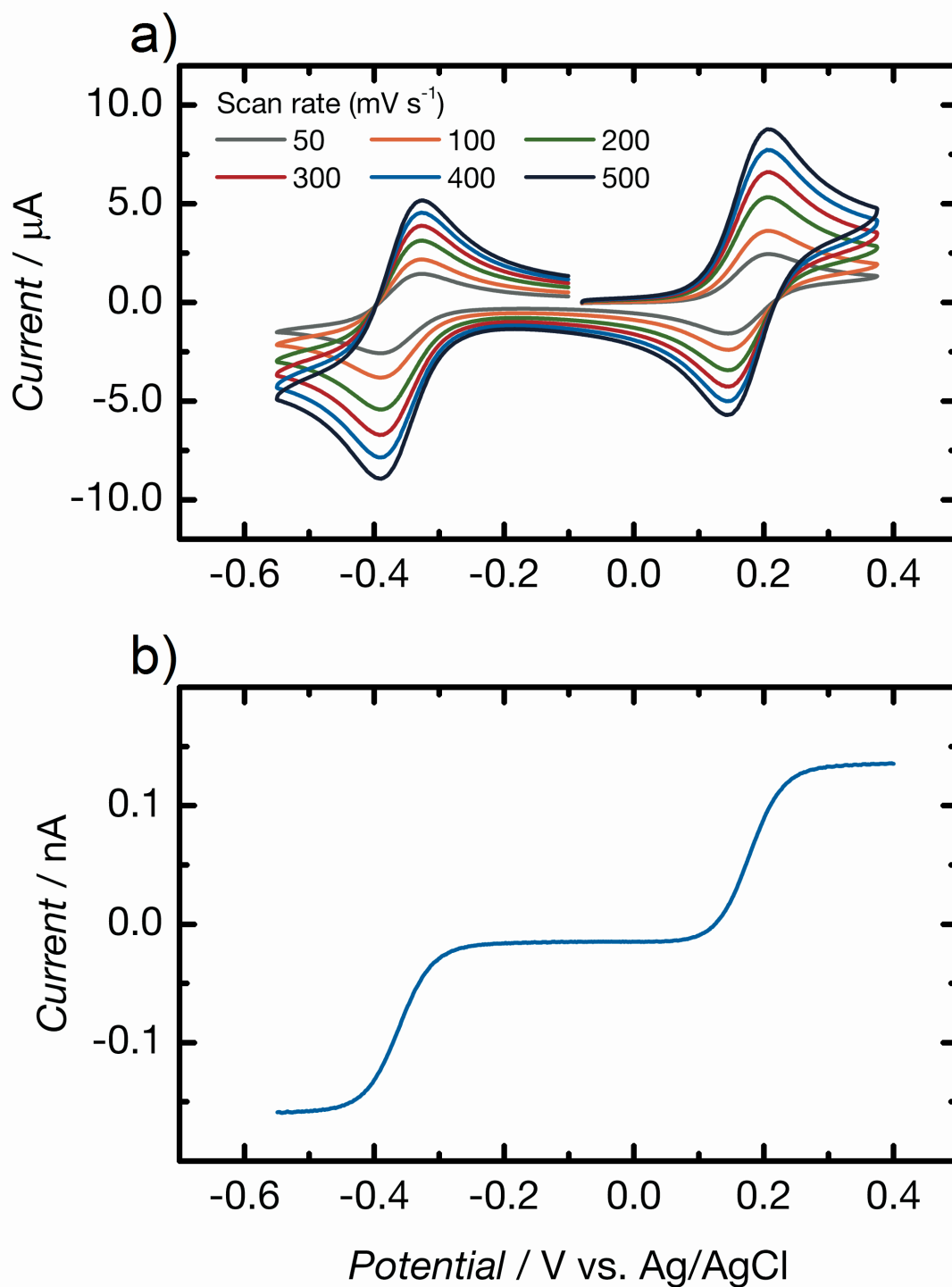


Figure S4: (a) Transient cyclic voltammograms obtained when chemically synthesized [Pt(NH₃)₄](TCNQ)₂ (**2**) (from water) is dissolved in acetonitrile (0.1 M Bu₄NPF₆) using a GC (1.5 mm) electrode at designated scan rates. (b) Steady-state voltammogram of the same solution obtained with a 10 μm Pt micro-disk electrode at scan rate of 20 mV s^{-1} .

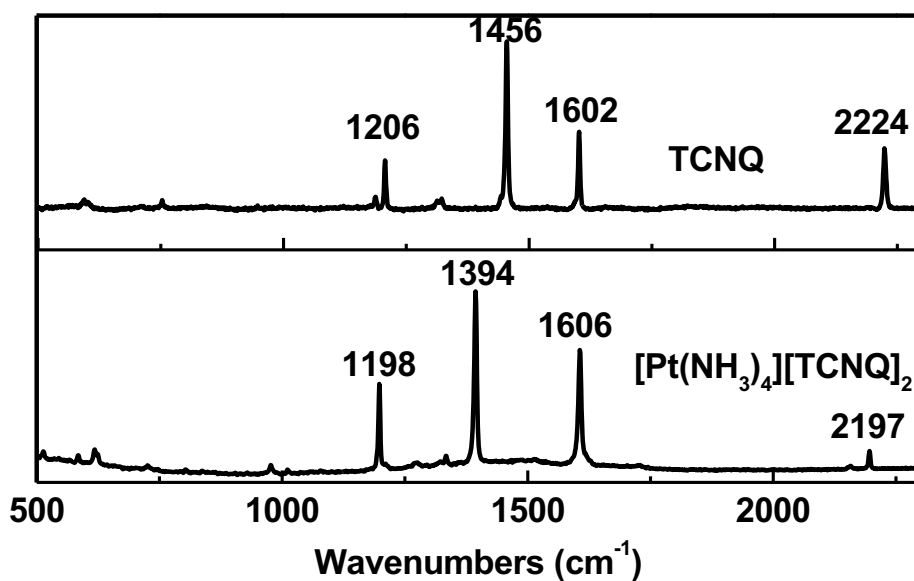


Figure S5: Raman spectra of solid TCNQ and solid [Pt(NH₃)₄][TCNQ]₂ (**2**) collected after reductive electrolysis (15 min) at $E_{app} = -0.15$ V when a TCNQ-modified ITO electrode (mechanical attachment method) is in contact with aqueous 0.10 M [Pt(NH₃)₄](NO₃)₂ electrolyte.

Voltammetric Evidence of a Nucleation/Growth Mechanism for the TCNQ|[Pt(NH₃)₄](TCNQ)₂ solid-solid state interconversion

Cyclic voltammetry provides support for the presence of rate-determining nucleation-growth kinetics^{S2-12} in the electrochemically induced TCNQ|[Pt(NH₃)₄](TCNQ)₂ solid-solid state interconversion processes. This is provided by the detection of current loops (Figure S9) in the cyclic voltammograms as can be detected upon reversing the direction of the scan at foot of reduction process when a TCNQ modified electrode is in contact with 0.1 M [Pt(NH₃)₄]²⁺ aqueous electrolyte.

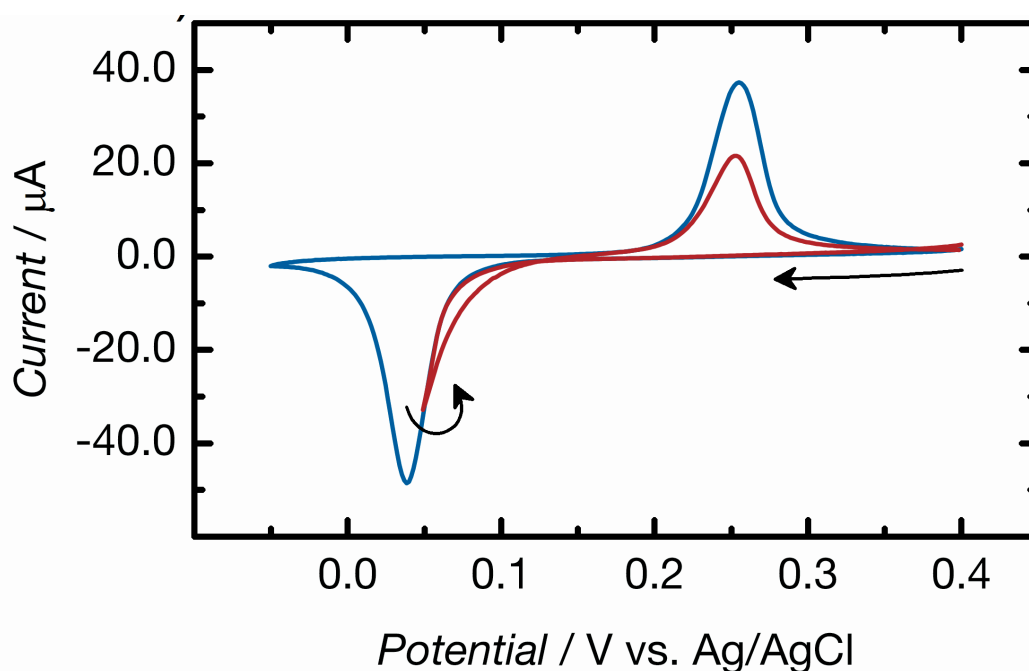


Figure S6: Cyclic Voltammograms obtained under same conditions as in (a) but at a scan rate of 20 mV s⁻¹, and for the fourth and fifth cycles with the potential switched at the foot of the reduction wave, which induces a hysteresis loop (as indicated by an arrow).

Chronoamperometric Evidence of a Nucleation/Growth Mechanism

Additional evidence for nucleation/growth kinetics can be obtained from analysis of current-time (i - t) data obtained from double potential step chronoamperometric experiments. Figure S7 shows a chronoamperogram obtained by stepping the potential from an initial value ($E_i = 350$ mV), where no faradaic current is present, to a more negative value ($E_{\text{red}} = -50$ mV) that allows reduction of TCNQ into TCNQ^{1-} along with concomitant interaction with $[\text{Pt}(\text{NH}_3)_4]^{2+}_{(\text{aq})}$ to form $[\text{Pt}(\text{NH}_3)_4](\text{TCNQ})_2$. After 20 seconds, the potential is stepped back to $E_{\text{ox}} = 250$ mV to induce oxidation of TCNQ^{1-} back to its neutral form, TCNQ. Current maxima characteristic for the presence of a rate-determining nucleation-growth process are clearly observed for both the reduction and oxidation components.

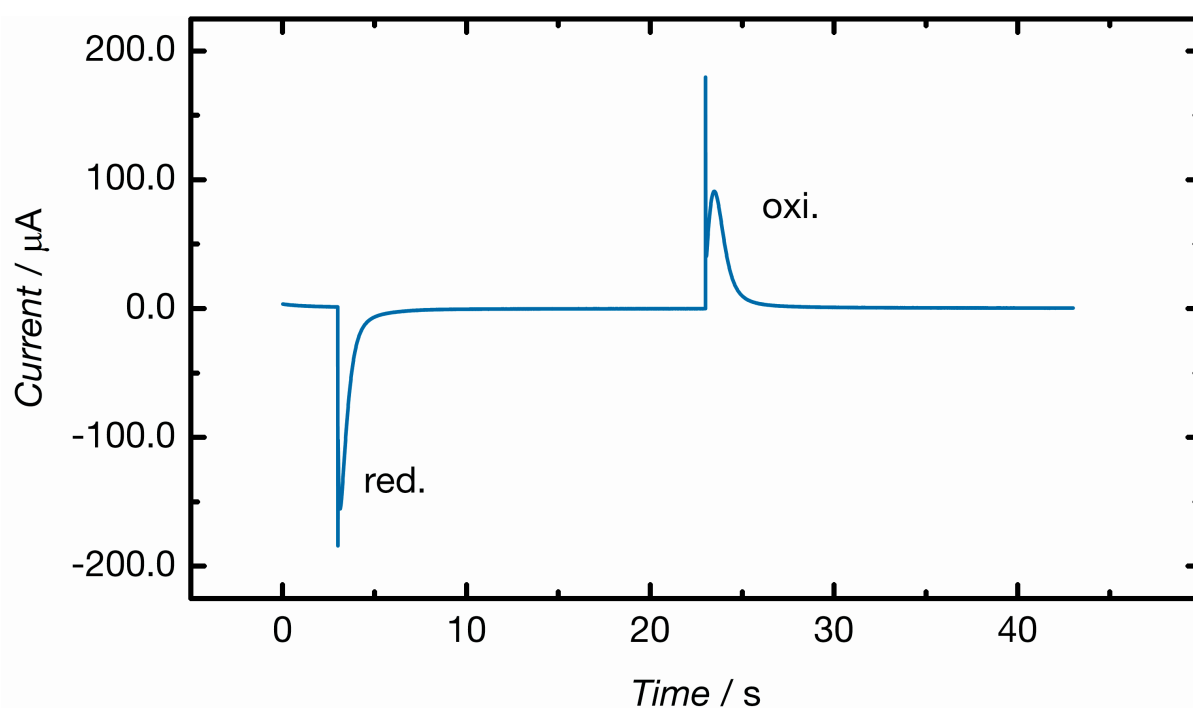


Figure S7: I - t chronoamperometric transient obtained when a GC electrode modified with TCNQ (mechanical attachment method) is placed in contact with aqueous 0.1 M $[\text{Pt}(\text{NH}_3)_4](\text{NO}_3)_2$ electrolyte and the potential is stepped from $E_i = 350$ to $E_{\text{red}} = -50$ mV for 20 s to induce reduction and then back to $E_{\text{ox}} = 250$ mV to induce oxidation.

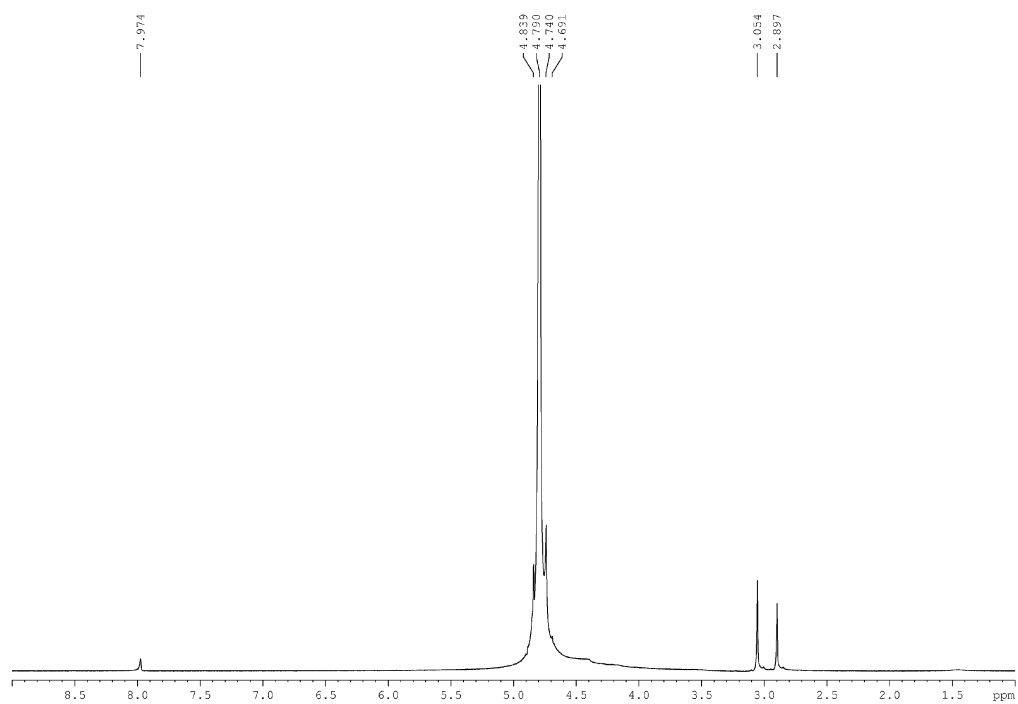


Figure S8: The ^1H NMR spectrum of the supernatant following soaking a crystal of $[\text{Pt}(\text{NH}_3)_4](\text{TCNQ})_2 \cdot (\text{DMF})_2$ (**1**) in D_2O after for ~ 30 mins.

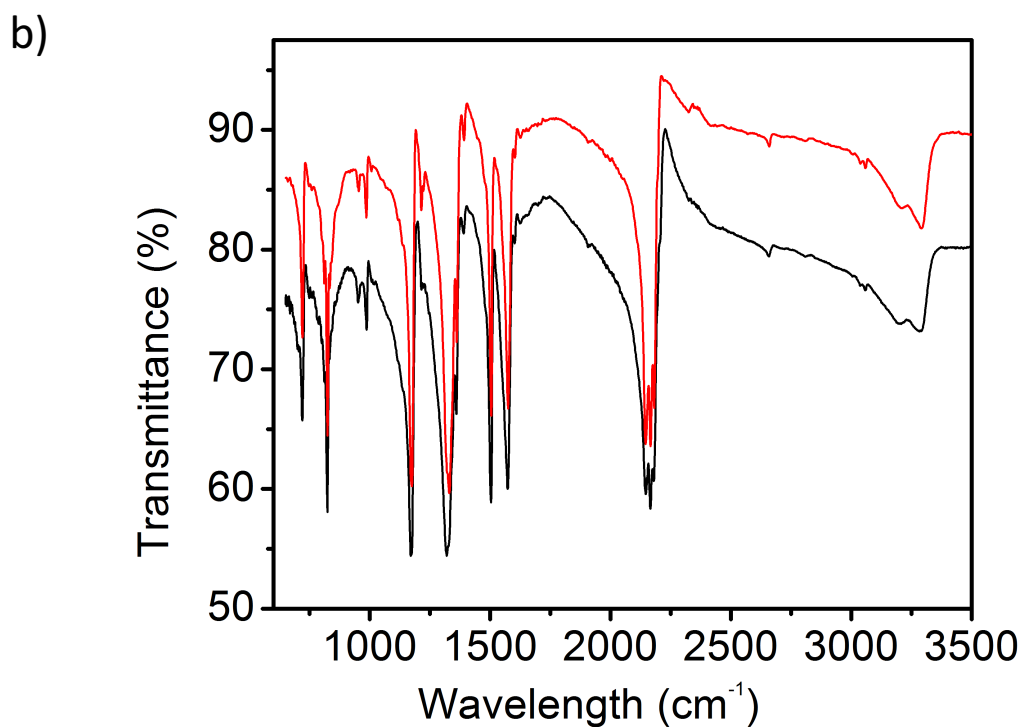
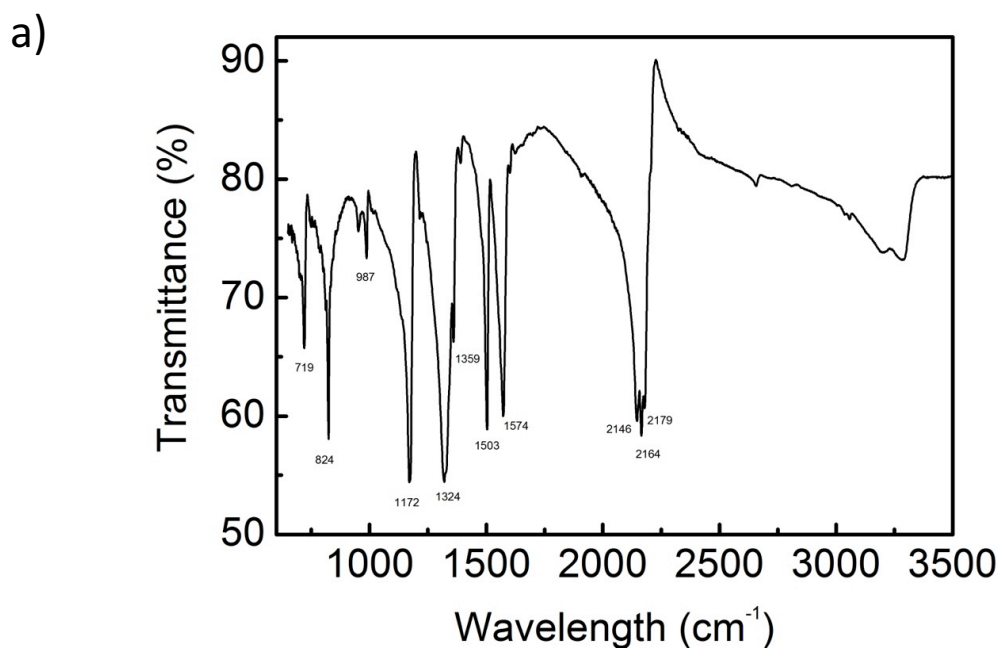


Figure S9: (a) FTIR of a crystal of $[\text{Pt}(\text{NH}_3)_4](\text{TCNQ})_2 \cdot (\text{DMF})_2$ (**1**) after soaking for ~ 30 mins in D_2O , (b) Comparison of the FTIR of **2** (red) and **1** after soaking for ~ 30 mins in D_2O (black).

Table S1. Assessment of several TCNQ/TCNQF₄-derived compounds, in various redox level, to act as a catalyst for the redox reaction between thiosulfate anions and ferricyanide ions in aqueous solution. Reaction conditions are described in the main text and [13].

TCNQ(F ₄)	Redox level	Cation	Soluble in water	Catalytic activity	Ref.
TCNQ	0		✗	✗	This work
"	1-	Li ⁺	✓	✗	[13]
"	1-	Bu ₄ N ⁺	✗	✗	[13]
"	1-	[Pt(NH ₃) ₄] ²⁺	✗	✗	This work
TCNQF ₄	0		✗	✗	This work
"	1-	Li ⁺	✓	✓	[13]
"	1-	[Pt(NH ₃) ₄] ²⁺	✗	✓	[13]
"	2-	Li ⁺	✓	✓	This work
"	2-	Pr ₄ N ⁺	✗	✓	This work

Supplementary References

- S1. H. Endres, H. J. Keller, W. Moroni, D. Nothe and V. Dong, *Acta Crys. B*, **1978**, *34*, 1703-1705.
- S2. S.-I. Terashita, K. Nazumi, Y. Ozaki and S. Takagi, *J. Phys. Chem.*, **1995**, *99*, 3618-3628.
- S3. F. H. Herbstein and M. Kapon, *Crystallogr. Rev.*, **2008**, *14*, 3-74.
- S4. P. G. Gucciardi, S. Trusso, C. Vasi, S. Patane and M. Allegrini, *Phys. Chem. Chem. Phys.*, **2002**, *4*, 2747-2753.
- S5. A. Nafady, A. P. O'Mullane, A. M. Bond and A. K. Neufeld, *Chem. Mater.*, **2006**, *18*, 4375-4384.
- S6. A. Nafady and A. M. Bond, *Inorg. Chem.*, **2007**, *46*, 4128-4137.
- S7. A. M. Bond, S. Fletcher, F. Marken, S. J. Shaw and P. G. Symons, *J. Chem. Soc., Faraday Trans.*, **1996**, *92*, 3925-3933.
- S8. A. M. Bond, S. Fletcher and P. G. Symons, *Analyst*, **1998**, *123*, 1891-1904.
- S9. M. Oyama, R. D. Webster, M. Suarez, F. Marken, R. G. Compton and S. Okazaki, *J. Phys. Chem. B*, **1998**, *102*, 6588-6595.
- S10. A. Nafady, A. M. Bond and A. Bilyk, *J. Phys. Chem. C*, 2008, *112*, 6700-6709.
- S11. A. Nafady, A. M. Bond, V. Qu and L. L. Martin, *J. Solid State Electrochem.*, **2013**, *17*, 1609-1620.
- S12. A. Nafady, A. M. Bond and A. P. O'Mullane, *Inorg. Chem.*, **2009**, *48*, 9258-9270.
- S13. J. Lu, B. F. Abrahams, B. Winther-Jensen, L. L. Martin and A. M. Bond, *ChemCatChem*, **2014**, *6*, 2345-2353.